Fleri Jesse (Orcid ID: 0000-0002-3824-9915)

Nardin William (Orcid ID: 0000-0002-5490-879X)

Empirical observations and numerical modelling of tides, channel morphology, and vegetative effects on accretion in a restored tidal marsh.

Jesse R. Fleri[1,2], Sara Lera[2,3], Alessandro Gerevini[2,4], Lorie Staver[2], William Nardin[2]

[1] Department of Forestry and Conservation Sciences, University of British Columbia, Vancouver, BC, Canada

[2] Horn Point Laboratory, University of Maryland Center for Environmental Science, Cambridge, MD, USA

[3] Department of Civil, Constructional and Environmental Engineering, University of Rome "La Sapienza", Rome, Italy

[4] Department of Engineering and Architecture, University of Parma, Parma, Italy

Running Header: Tidal marsh sediment dynamics

*Corresponding author.

Email address: jessefleri@gmail.com (Fleri, J.R.)

This article has been accepted for publication and undergone full peer review but has not been through the copyediting, typesetting, pagination and proofreading process which may lead to differences between this version and the Version of Record. Please cite this article as doi: 10.1002/esp.4646

Abstract

Tidal marshes form at the confluence between estuarine and marine environments where tidal movement regulates their developmental processes. Here, we investigate how the interplay between tides, channel morphology, and vegetation affect sediment dynamics in a low energy tidal marsh at the Paul S. Sarbanes Ecosystem Restoration Project at Poplar Island. Poplar Island is an active restoration site where fine-grained material dredged from navigation channels in the upper Chesapeake Bay are being used to restore remote tidal marsh habitat toward the middle bay (Maryland, USA). Tidal currents were measured over multiple tidal cycles in the inlets and tidal creeks of one marsh at Poplar Island, Cell 1B, using Acoustic Doppler Current Profilers (ADCP) to estimate water fluxes throughout the marsh complex. Sediment fluxes were estimated using acoustic backscatter recorded by ADCPs and validated against total suspended solid measurements taken on site. A high-resolution geomorphic survey was conducted to capture channel cross sections and tidal marsh morphology. We integrated simple numerical models built in Delft3d with empirical observations to identify which eco-geomorphological factors influence sediment distribution in various channel configurations with differing vegetative characteristics. Channel morphology influences flood-ebb dominance in marshes, where deep, narrow channels promote high tidal velocities and incision, increasing sediment suspension and reducing resilience in marshes at Poplar Island. Our numerical models suggest that accurately modelling plant phenology is vital for estimating sediment accretion rates. In-situ observations indicate that Poplar Island marshes are experiencing erosion typical for many Chesapeake Bay islands. Peak periods of sediment suspension frequently coincide with the largest outflows of water during ebb tides resulting in large sediment deficits. Ebb dominance (net sediment

export) in tidal marshes is likely amplified by sea-level rise and may lower marsh resilience. We couple field observations with numerical models to understand how tidal marsh morphodynamics contribute to marsh resilience.

Keywords: Delft3D, ADCP, tidal marshes, channel dynamics, numerical modelling

Introduction

Tidal marshes provide a wide variety of supportive, provisional, regulatory, and cultural ecosystem services (Barbier et al., 2011). Specifically, tidal marsh ecosystems sequester pollutants, promote biodiversity, buffer coastal infrastructure against large storms, encourage recreation and tourism and are increasingly recognized as globally significant blue carbon sinks (Barbier et al., 2011; Fourqurean et al., 2012). Chesapeake Bay fisheries are widely supported by these highly productive environments yet there is a struggle to acquire adequate funding for marsh research and conservation (Boesch 1984; UNEP 2006). Despite their local and global significance, a quarter to half of all tidal marshes on earth have disappeared (Deegan et al., 2012, Millennium Ecosystem Assessment 2005). Conservative projections of global sea-level rise forecast a minimum rise of 0.52 m before 2100 and emphasize that those changes will not occur uniformly across oceans (Parry et al., 2007). Recent models project a maximum rise of 0.64 m in the Chesapeake Bay by 2050, and 1.74 m by 2100 (National Research Council 2012). Receding shorelines would have devastating impacts on coastal infrastructure, commerce, aquatic ecosystem services and resilience.

Resilience can be characterized by the ability of an ecosystem to rebound after a disturbance event (e.g., hurricanes and drastic sea-level rise). Aquatic ecosystems are generally thought to be moderately resilient under dynamic climate regimes (Bernhardt and Leslie, 2013). However, unprecedented warming and sea-level rise at rates three to four times higher than the global average appear to be testing the natural resilience of Chesapeake Bay ecosystems (Sallenger et al., 2012). In recent decades, 13 low relief Chesapeake Bay islands have been lost to inundation and erosion, while hundreds of thousands more acres of tidal marsh habitat are predicted to disappear (Glick et al., 2008; Craft et al., 2009). Some developed Chesapeake Bay islands have been entirely abandoned while other communities persist by armoring their shorelines to limit erosion; substantially less is being done to protect ecologically significant habitat surrounding these islands.

Efforts have recently been made to better understand the developmental processes driving tidal marsh formation (Mudd et al., 2004). The geomorphic and biotic dynamics that lead to the creation of tidal marsh islands under controlled, artificial, and in-situ conditions have previously been investigated (Fagherazzi et al., 2012; Kirwan et al., 2007; Temmerman et al., 2005; Morris et al., 2002). These experiments generally demonstrate a negative correlation between vegetation density and canopy flow, i.e. turbulence (Leonard and Luther, 1995; Leonard and Croft, 2006). It is well established that aquatic vegetation modifies flow fields and is capable of dissipating wave energy (Anderson et al., 2014; Nardin et al., 2018). Vegetative traits such as leaf area and stem diameter can influence roughness which, in turn, can alter attenuation of low energy waves and sediment deposition rates (Ward et al., 1984). The magnitude of roughness and the associated changes to waves are a function of the modelled vegetation. Widespread taxa such as

Spartina spp are often chosen for tidal marsh models due to their prevalence in marshes and ecological significance. Relatively little research has examined the role of vegetation in the aggregation and erosion of mineral sedimentation in tidal marshes (Baustian et al., 2012). Previous studies used idealized numerical modeling to show how vegetation density and channel morphology change tidal flow in mangrove forests (Bryan et al., 2017), arid intertidal systems (Kearney and Fagherazzi, 2016) and in the evolution of delta mouth bars (Nardin et al., 2013; Nardin and Edmonds, 2014; Lera et al., 2019). These works suggest that shallow water vegetation, similar to tidal marsh vegetation, would increase the frictional effect vegetation has on tidal currents; thereby inducing sediment trapping. If numerical models are expected to simulate real world environments and inform management decisions with accuracy, similarly complex models must be developed for each ecosystem (Nardin et al., 2016).

Coastal islands and tidal wetlands are being subjected to an unprecedented degree of inundation and erosion that is resulting in their widespread disappearance (Crosby et al., 2016). An active attempt to conserve and restore these ecosystems is underway but has been insufficient to compensate for the area lost. Ecological restoration has long been considered an “acid test” for ecology (Bradshaw, 1984), where restoration practitioners test how well the scientific community truly understands the complexities involved in ecosystem formation. In many cases, restoration projects are not as successful as practitioners would like, with most projects lacking adequate funding to afford post project monitoring or fail to include criteria for measuring success (Suding, 2011). Improved understanding of sediment dynamics in low profile tidal marshes would help improve conservation prioritization

models and redirect resources toward areas with the highest potential impact and chances of long-term restoration success.

We seek to characterize the hydrologic and geomorphic regimes present in a portion of restored *Spartina alterniflora* tidal marsh at the Paul S. Sarbanes Ecosystem Restoration Project at Poplar Island (Poplar Island), Maryland. In this study, we used in-situ field measurements of tides, vegetation, and channel morphology to inform an investigation into the factors that influence sediment transport and flood-ebb dominance in the system. Specifically, we define an ebb dominated system as having a net loss of sediment while flood dominance describes a marsh complex that captures sediment and promotes vertical accretion (Brown and Davies, 2010). We complemented these observations by building hydro-geomorphic numerical models in Delft3D to systematically evaluate the role of vegetation with stand characteristics that imitate the effect *S. alterniflora* has on tidal marsh development. By modelling simple channel configurations in a vegetated platform with varying channel depths, widths, and vegetative characteristics, we can assess how these factors interact to determine ebb-flood dominance in tidal marshes. Lastly, we characterize the morphological implications of different channel-vegetation scenarios and their significance for tidal marsh accretion and resilience.

Materials and Methods

Study site

Poplar Island is an active ecosystem restoration site constructed of sediment that is dredged from the navigation channels approaching Baltimore Harbor to restore remote island habitat in the Chesapeake Bay. Spanning 5.6 km by 0.8 km, Poplar Island is representative of numerous islands throughout the region (Fig. 1a)

that have been subjected to severe erosion and inundation by rising sea levels. Originally 461 ha, Poplar Island had degraded to approximately 1.6 ha before a collaborative effort between the Maryland Department of Transportation, Maryland Port Administration, Maryland Environmental Service and the U. S. Army Corps of Engineers began an effort to restore the island in 1998 (Fig. 1b). The island is subdivided into containment cells, half of which will be tidal marsh and half upland habitat when the project is complete (Fig. 2a). As of May 16, 2017, 24.47 Million Cubic Meters (MCM) of fine-grained (median sand <10%, Stevenson et al., 2013) dredged materials have been placed on Poplar Island, totaling 694 ha of restored mixed upland and wetland habitat (Kelly W., 2017). Our measurements come from a single tidal marsh, Cell 1B, with neighboring marshes connected by two channels, one to the North (NE) and one to the South (SE), and two adjacent 1.8 m^2 box culverts that connect the marsh to the Chesapeake Bay (Fig. 2b). Cell 1B was graded and opened to tidal exchange in 2011 and planted with nursery gown *S. alterniflora* (low marsh) and *S. patens* (high marsh) in 2012. The mean great diurnal tide range (difference between mean higher high water (MHHW) and mean lower low water (MLLW)) at this site is 0.468 m (Kent, 2015). Target elevations were: high marsh 0.75 m above MLLW, low marsh 0.57 m above MLLW, with flooding typically occurring twice per day in the low marsh and once per day in the high marsh. Preliminary surveys and hydrodynamic modelling in and around Poplar Island have provided a useful, but incomplete picture of the environmental forces sculpting the marsh complex.

Tidal flux

We simultaneously deployed Nortek Aquadopp Acoustic Doppler Current Profilers (ADCP) in the marsh's three channel inlets in early July and deployed the same three ADCP instruments throughout the tidal marsh interior in mid-July (Fig. 2). ADCPs are acoustic based instruments that measure acoustic backscatter at varying water column depths and have been a well-established method of estimating suspended solid concentrations (SSC) and net sediment transport (Holdaway et al., 1999; Gartner, 2004). ADCP units were deployed under a variety of resolutions at different locations (Table 1). Instruments recorded every 3 minutes at 1-2 MHz, averaged over 60 seconds, and at height intervals (cell size) of 5, 10, or 25 cm. Water depths were calculated from pressure values recorded by ADCPs and validated against depth measurements taken with meter sticks (Fig. 3). SSC was calculated from backscatter intensity measurements using the *Lohrmann, 2001* equation (Eq. 4). SSC estimates were validated against total suspend solid (TSS) measurements taken from ISCO autosamplers deployed alongside each ADCP unit, sampling hourly during the first 24 hours. ADCPs were bottom mounted on weighted PVC or metal plates and placed approximately at the center of each channel, roughly corresponding to thalweg (Monismith, 2005). ISCOs were deployed 5-10 m away from ADCP units near the thalweg to avoid disturbing waterflow, except at the culvert (CUL) where the ISCO probe was two to three meters from the profiler. All ADCPs were deployed with the transducer head pointed into the tidal marsh, making the interior-oriented velocities a reasonable estimate of tidal fluxes.

Sediment fluxes (q) were computed as concentration (c) times velocity (u) times the cross-sectional area (A) of the flow. Where subscript i denotes an instantaneous measurement.

$$q_i = c_i u_i A_i \quad (1)$$

Equation (1) provides the ability to calculate flux at discrete time steps. Applying an averaging period based on tidal cycles and summing *n* measurements over that period, net tidal flux ($\bar{q}$) can be calculated.

$$\bar{q} = \sum_i^n q_i \Delta t \quad (2)$$

Cross-sectional area at the main culvert was calculated by multiplying the fixed channel width by water depth at three-minute intervals. Irregular channel areas were calculated using the mean-section method where (d_1) is the depth from water level to the surface at point 1, (d_2) is depth at point 2, and (w) is the distance between points d_1 and d_2 which was standardized at 0.5 m. Total area (A) is the sum of partial section areas (A_x).

$$A_x = [\frac{(d_1 - d_2)}{2}]w \quad (3)$$

Sediment flux

ADCPs record backscatter intensity (BI) on a 0 to 255 count scale. We converted these values using a version of the applied sonar equation (Deines, 1999) found in the R package 'oce' (Version 0.9-21), where BI is converted to SSC in decibels by multiplying count by 0.43. Modifications were made to account for signal loss due to spherical spreading and water absorption (Fisher and Simmons, 1977) while particle attenuation was ignored due to relatively low salinity levels (Lohrmann, 2001).

$$SCC\ (db) = Amp * 0.43 + 20log10(r) + 2\alpha_w r \quad (4)$$

ADCP measurements of SSC are reliant on sediment being the primary constituent in the water column. The ISCO took hourly samples of bottom water, 30-40 cm above the seafloor, to estimate sediment particle size and percent organic matter for our numerical models. Using an ISCO sampler allowed for the calibration of backscatter intensity and provided a second line of evidence to support the validity

of backscatter calculations. Organic content was determined by loss on ignition (Heiri et al., 2001).

Vegetation and cross section survey

Line transects were established at angles perpendicular to measured channels where vegetation was sampled. Vegetation consists primarily of *S. alterniflora*. Measurements of stem density, canopy height, and stem diameters were recorded at 20 m intervals using 0.1 m^2 quadrats (Fig. 4). Stem densities were determined by counting each stem inside the quadrat. Mean stem diameter was calculated from measurements taken on ten stems per quadrat at a height of 15 cm from the soil surface using a Vernier caliper. Canopy height was determined by averaging the heights of the five tallest individual stems within each quadrat. Vegetative characteristics were used to characterize stand features in our numerical flow model built in Delft3D.

Channel cross sections were measured within the marsh complex using a Topcon Hiper V GPS GLONASS L1 L2 RTK. The RTK georeferenced depth points in NAVD88 datum, allowing us to empirically determine channel shape and depth for model construction. The instrument's base was placed on known coordinates (Poplar Island benchmark CM 2: https://www.ngs.noaa.gov/NGSDataExplorer/) located on the western side of Cell 1B (Fig. 2b). Within the tidal marsh area, we used a rover receiver mounted on an extendable pole to survey channel elevation.

Numerical model setup

We configured a numerical model to replicate the geomorphic characteristics of an interior channel (SC). We focused our modelling on SC because it is located

deep inside of the marsh complex and away from the actively eroding marsh edge. All numerical models were built using Delft3D to simulate the hydrodynamic and morphodynamic processes acting during flood-ebb tidal cycles. Our models were tested under a range of configurations to understand how the presence and density of tidal marsh vegetation influenced channel development over time. Delft3D allows users to create two- and three-dimensional models that accurately simulate geomorphic development. We conducted a sensitivity analyses to determine the most informative configuration for our investigation. We found that using a depth-averaged model (2D) was less computationally intensive and produced very similar results when compared to alternative 3D approaches. As a result, all future references to numerical models assume a 2D configuration.

Our models were built on a 0.09 km^2 numerical domain with a 100 m long channel running through the center (Fig. 5a). Our model grid was built using 6 m^2 cells, with a high-resolution refinement of 2 x 6 m along the centerline. Two resolutions were selected to optimize run time and data restitution accuracy. We simulated three equal area channels with unique morphologic features to examine channel evolution (Fig. 6). Model one simulates fluid flow and sediment transport based on the observed features at SC. Models two and three represent idealized scenarios with deep, narrow channels (6 x 0.8 m) and shallow, wide channels (24 x 0.245 m).

Simulated tidal channels are incised into an erodible coastline where no flux boundary condition is imposed and the mean water level is zero. Water level boundary conditions were set to replicate measured sea-level variation (i.e. tides) from the open basin (Fig. 5b). The simulated tide is semidiurnal and approximates in-

situ Chesapeake Bay conditions (Fig. 5c). Bathymetric variation was limited by assigning equal bed elevations to the open basin and channel thalweg.

Bottom roughness was modeled using Chézy's formula with a constant value (C_b) of 65 $\sqrt{\mathrm{m}}/s$. We satisfy Courant-Frederichs-Levy's numerical stability criteria by using a time step of 0.2 min (*Lesser et al.*, 2004). Horizontal eddy viscosity was set equal to a uniform value of 0.001 m^2/s and the horizontal eddy diffusivity was set at 10 m^2/s. We reduce modelling error by setting a 180 min spin-up interval that allowed the hydrodynamics to stabilize prior to allowing morphological updating.

Sediment boundary conditions were set to continuously supply suspended silts with a grain size of 20 µm. We focused on modelling cohesive sediment transport because our ISCO field surveys showed that non-cohesive sediment made a very limited contribution to SSC. As a result, we imposed a seaward sediment boundary condition with a constant input of 0.64 kg/m^3, similar to *Nardin et al.,* 2013. All sediment was characterized by reference density of hindered settling of 1600 kg/m^3 specific density of 2,650 kg/m^3, dry bed density of 800 kg/m^3 and a settling velocity of 0.001 m/s converted using methods from *Van Rijn, 1993.*

We simulated tidal marsh vegetation at all points in the modelling domain where flow equaled zero (high marsh) and along channel banks. We modelled vegetation with six unique combinations of stem density (n = 2, 6, 10) and height (h_v = 0.1, 1.6 m) based on field observations *(*Table 2a). Vegetation heights were chosen to represent winter (h_v = 0.1 m) and summer (h_v = 1.6 m) growing conditions. By simulating submerged and emergent vegetation, we can examine how suspended sediments interact with vegetation during different seasons to understand how plant phenology affects sediment behavior and tidal marsh accretion.

Vegetation model

Vegetation substantially reduces tidal flow (e.g. Liu et al., 2003; Mazda et al., 1997; Temmerman et al., 2005; Wu et al., 2001), due to enhanced frictional drag caused by stem and leaf characteristics which can be modelled in Delft3D. Frictional drag is expressed as an effect on hydraulic bed roughness and flow resistance. Delft3D incorporates vegetation effects by allowing users to specify roughness classes.

Vegetation was modelled using equations proposed by *Baptist et al.,* 2005, which represents marsh grasses as rigid cylindrical stems characterized by height (h_v), diameter (D), density (n) and a drag coefficient of the vegetation structure (C_D). In the presence of fully emergent vegetation (vegetation taller than water depth), the flow velocity profile is constant beneath the surface. In contrast, submerged vegetation (vegetation below than water depth) develops a constant velocity profile from the base of the channel to the top of the stems. A logarithmic velocity profile is then fitted from the top of the submerged vegetation to the water surface.

We first applied the Baptist equation to the submerged vegetation simulation, where the Chézy friction value for fully submerged vegetation (C_{rs}) is calculated by deriving n from $n = mD$ (where m is the number of stems per square meter and D is the stem diameter), k is the Von Karman constant, g is acceleration due to gravity and C_b is the bed roughness according to Chézy.

$$C_{rs} = \frac{1}{\sqrt{\frac{1}{C_b^2} + \frac{C_D n h_v}{2g}}} + \frac{\sqrt{g}}{k} ln\left(\frac{h}{h_v}\right) \quad (5)$$

When modelling emergent vegetation, we removed the logarithmic growth term and assumed a constant vertical velocity profile that results in a simplified Chézy friction value (C_r):

$$C_r = \frac{1}{\sqrt{\frac{1}{C_b^2} + \frac{C_D nh}{2g}}} \quad (6)$$

Data Analysis

To better understand the relationship between sediments and vegetation, we calculated a sediment concentration ratio (R_c). R_c is an estimate of the potential volume of suspended sediment trapped by vegetation across the simulated high marsh during the last four tidal cycles. Positive R_c values indicate that sediment is less able to settle due to the presence of vegetation. SSC_{veg} and $SSC_{no\ veg}$ are determined by estimating the total suspend sediment in the water column at the end of each simulation.

$$R_c = \frac{SSC_{veg} - SSC_{no\ veg}}{SSC_{no\ veg}} \quad (7)$$

Coupling the hydrodynamic and morphodynamic models allowed us to further investigate sediment dynamics within our modelled marsh configurations. For that reason, we calculated a sediment accretion ratio (R_a):

$$R_a = \frac{BL_{veg} - BL_{no\ veg}}{BL_{no\ veg}} \quad (8)$$

R_a is a comparative term that estimates bed level change in the designated "high marsh" zones between vegetated and non-vegetated simulations. BL_{veg} is the net change in bathymetry when vegetation is present, while $BL_{no\ veg}$ represents non-vegetated cases. Positive R_a values indicate that marsh accretion occurs more rapidly when marsh vegetation is present. Both R_c and R_a are calculated as averaged values across the vegetated marsh platform and exclude the channels (Table 2b).

Results

Water fluxes and tidal symmetry

Multiple low and high tide events were recorded during this study. We regularly observed the strongest tidal currents during ebb tides (Fig. 7). The magnitude of ebb tides varied but were never weaker than their associated flood tide at any of the three inlets. We therefore classified this tidal marsh as having an asymmetric tide that is ebb dominant (i.e. stronger ebb tides).

We compared water fluxes at each of the three inlets entering our study site which allowed us to determine that water is primarily exchanged through the culverts (CUL) (Fig. 3b). Water fluxes at the NE inlet were near zero (median = 0.04 m^3/s) for the first deployment and did not greatly contribute to interconnectivity between wetland cells. Median positive and negative fluxes were 11 and 19 times lower than those measured within CUL. Water fluxes in the SE inlet (median = 0.21 m^3/s) were observed to be greater than those in the NE inlet but substantially lower than CUL with positive and negative fluxes being 4 and 10 times less. CUL fluxes during ebb tides had a median value of -2.07 m^3/s while flood tide fluxes had a median of 1.15 m^3/s.

Flood-ebb dominance

Field observations provide evidence of ebb dominance (net sediment export) at our study site. Sediment and water fluxes exhibited very similar distributional trends throughout both sampling periods (Fig. 3b-c). Only fluxes in the culvert (CUL and CUL2) were bimodally distributed while all other sites were characterized as having slightly skewed or normal distributions. Bimodality would be expected in channels

heavily influenced by flood and ebb tides. The semidiurnal structure of the tide diminished with distance from the culvert, as tidal currents are diffused by topography and vegetation. Normal distributions may be indicative of a diminished effect by tidal processes. Current directions ranging from ~ +50° to +90° represent flood tides and ~ −90° to −130° were classified as ebb tides within the culvert. Sediment fluxes in the culvert where similar during the ebb and flood tides with a median ebb value of - 0.083 kg/m^3 and 0.048 kg/m^3 during flood tides. Median ebb and flood sediment fluxes within the culvert were 3 to 8 times higher than those occurring in the main and secondary channels.

Water velocities were highest in the culvert during the ebb tide and reduced linearly from the surface to the channel bed. Flood tide velocities followed a similar, less noticeable trend. In contrast, *SSC* was observed to be most extreme during peak flood tides and during transitional periods while ebb tides generally had moderated *SSC* levels (Fig. 8d). *SSC* was more normally distributed during flood tides where moderate water depths had relatively low *SSC* observations. This trend emerged in both ADCP deployments at CUL under various weather conditions. Irregular velocity patterns were observed at both inlets, suggesting that external forces may be influencing marsh development at connecting points between neighboring marsh complexes (Fig. 8b-c). Additionally, water velocities and fluxes were relatively low inside MC and SC. External factors such as channel morphology, vegetation, and wind may have promoted additional mixing in this area. Velocity was lowest in MC and had the least variable *SSC* values. SC, however, had several periods where velocity magnitudes were unusually large but maintained the lowest observed *SSC* of all our ADCP sites with observations dropping below 50 dB. Sediment appears to drop out of the water column the further it travels from the

culvert. Coupling this observation with observed ebb tides having a higher *SSC* than flood tides, a case for ebb dominance can be established.

Modelled Tidal Hydrodynamics

Tidal flow is the main variable affecting flow circulation and hydrodynamics at Poplar Island. Field data suggests the existence of an asymmetric ebb dominant current that we sought to replicate using Delft3D FLOW. The main channel of Cell 1B (MC) was selected as a reference point for our numerical models. Hydrodynamic simulations at MC closely resembled tidal patterns measured by ADCPs during field deployments.

Plotting water level against depth averaged velocity allows for the comparison of flood and ebb current magnitudes at every stage of the semidiurnal tide. The longitudinal depth averaged velocity (y component) mimics the tides by decreasing during ebb and increasing during flood tides. The transverse velocity (x component) is so small that it can be neglected along the centerline and increases almost linearly moving toward the lateral side of the channel, where the vegetation height and density increase.

Flood and ebb current velocities ranged from 0.8-1.0 m/s and 1.0-1.1 m/s, respectively, indicating that the simulated tide is asymmetric and ebb dominant, similar to in-situ observations. We found that initial channel geometries significantly altered velocity during the flood tide. Shallow, wide channels experienced notably lower depth-averaged velocity when compared to deep, narrow channels or the modelled SC channel (Fig. 9a-b). We found that stem density had a relatively small effect on current velocity. In contrast, peak flood and ebb velocities within the channel nearly double in the presence of emergent vegetation (Fig. 9c-d).

Channel geometry significantly affects the suspended sediment delivered to the high marsh. When vegetation is simulated at a constant stem height and density, variation in channel morphology lead to substantial sediment concentration disparities (Fig. 10a). Low velocities in the shallow, wide channels result in relatively small R_c observations in the high marsh when compared to deep, narrow channels. Low current velocities allow sediment to settle throughout the marsh but limit the magnitude of scouring and erosion. Chanel morphology directly influences water column velocity, thereby indirectly affecting the capacity of currents to penetrate marsh vegetation.

SSC changed in direct relationship to tidal symmetry and water level (Fig. 10). Stem density only affected *SSC* when vegetation was emergent and had the SC morphology (Fig. 10b-c). Emergent vegetation creates hydraulic resistance to flow, causing a decrement in velocity and maximum bed shear stress. In contrast, simulating tidal marsh vegetation at 0.1 m with various stem densities does not produce any significant variations in *SSC*. Vegetation height is the most influential plant characteristic for predicting accretion rates in our models (Fig. 11).

For short vegetation (Fig. 11a) percent R_c increases exponentially as stem density increases, producing a 6.5% growth in *SSC*. Low stem densities (n=2) produce 1% more growth in *SSC* than non-vegetated simulations. Similarly, high stem densities (n=10) produce 7.5% more *SSC* than non-vegetated cases. In contrast, emergent vegetation (Fig. 11b) R_c increases toward a horizontal asymptote, generating only a 5% increase in *SSC* but trapping substantially more sediment as a whole. Low densities of emergent vegetation produce 91% more *SSC* than non-vegetated cases, whereas higher densities produce 96% more *SSC*. In other words, density has a slightly larger effect on *SSC* for short vegetation than for tall

vegetation. We fitted an exponential function (R^2=0.965) to stem height at 0.1 m and a logarithmic function (R^2=0.827) when height was 1.6 m. Submerged vegetation had a significant effect on R_c, where increasing stem density led to an associated increase in R_c. Emergent vegetation, according to the Baptist equation, should have a uniform velocity profile leading to more efficient sediment trapping. However, when vegetation height is 1.6 m the behavior of R_c changes substantially and gradually tends to reach a constant value. We found that emergent stem densities greater than n=6 are less important for accumulating sediments than previously thought. We observed a slight decreasing trend in R_c when we simulated stem densities of n=8 and n=10.

Our models suggest that vegetation obstructs the movement of both water and sediment, thereby reducing *SSC* as material is allowed to settle during low velocity periods. R_a was correlated with increased channel width and vegetation volume (plant height x stem density) (Fig. 12). Vegetation was found to inhibit sediment accretion at large volumes and suggests that an optimum ratio of stem height and density exists for resilient tidal marshes (Fig. 12b).

Discussion

Channel morphology and plant phenology profoundly affect flood-ebb dominance in tidal marsh ecosystems (Carr et al., 2018). Our numerical models demonstrate the impact channel design and vegetation has on the long-term stability and resilience in marsh habitat. We found that dense, submerged vegetation and wide, shallow channels generally minimized peak tidal velocities and promoted marsh accretion more quickly. R_c and R_a were based only on SSC estimates from the high marsh which allowed for direct comparisons between vegetated and bare

channel simulations. We observed the R_a coefficient to be inversely related between submerged and emergent vegetation. Dense, submerged vegetation appears to promote sediment deposition while dense, emergent vegetation limits deposition. We posit that higher stem densities hinder flows from spreading throughout the marsh and releasing suspended sediment (Leonard and Reed, 2002). However, more in depth studies are needed to validate this observation. Nevertheless, these results are consistent with modelling studies in other vegetated environments (Nardin et al., 2016). Sediment deposition and marsh accretion is vital for long term restoration success and should be prioritized if future dredge islands are expected to persist.

Our field observations suggest that sediment is being exported from the Poplar Island's Cell 1B tidal marsh (Fig. 7 and 8). Net sediment fluxes at the culvert and main channel were negative, indicating the export of suspended sediments. In contrast, the secondary channel had a positive net flux, where sediments were accumulating. It is not unusual for marsh complexes to have spatially heterogeneous characteristics that lead to sediment eroding and aggregating non-uniformly (Moffett et al., 2010) between and across channels. Sediment was unable to accumulate at the seaward edge of the tidal marsh but increased with distance from the culvert, suggesting that wave energy may be less formative for interior marsh morphology. Sediment fluxes within the secondary channel exhibited greater variability than those of the main channel but were observed to have lower SSC. Tidal energy has a strong developmental influence on channel morphology and flood-ebb dominance that dissipates as water moves deeper into the tidal marsh interior and over vegetated surfaces (Möller et al., 2014). In low energy channels non-cohesive sediments are allowed to settle along banks and on the marsh platform. In contrast, high velocity flows near the culvert erode channel banks in the root zone, a process

called root scalping, and pull suspended particles out of the marsh complex (Priestas et al., 2015; Leonardi et al., 2016).

In addition to negative net sediment fluxes at our study site, we are concerned by the lack of incoming sediment from the Greater Chesapeake Bay. Tidal marshes are unlikely to persist where sea levels are projected to rise quicker than their platform (Morris et al., 2002). Ebb dominance compounds the effect of sea level rise by reducing platform height and destabilizing banks.

The greatest concentration of suspended sediments was observed at the culvert during peak ebb tides, suggesting that sediments are being exported from the marsh interior into the Chesapeake Bay. *SSC* for both inlets were observed to be net positive at much smaller scale, indicating a degree of inter-wetland connectivity and sediment import. Cell 1B is characterized by a minor ebb-asymmetry and ebb dominant conditions. These findings suggest that poor sediment retention should be considered a threat to ecosystem stability. While tidal inputs cannot be altered without reconstructing culverts in this wetland, future research may consider monitoring sediment transport at multiple wetland cells simultaneously to limit confounding spatiotemporal factors and better understand sediment fluxes.

Although we still have an incomplete understanding of the forces driving tidal marsh resilience, our study demonstrates that channel design and vegetation development are crucial factors for restoring tidal marsh habitat. *Belliard et al., 2016* suggests that vegetative effects on sediment deposition could be sufficient for tidal marshes to withstand low amounts of sea level rise, but at moderate to high levels (>10 mm/yr) numerical models predict marsh degradation. It is therefore imperative that restoration actions and contemporary modelling frameworks improve quickly enough to accommodate our most severe sea-level rise projections. The channels at

Poplar Island do not appear to be adequately designed to promote geomorphic marsh resilience. We observed a relatively low amount of sediment re-entering our study area after removal during ebb tides. We show that vegetation and channel stability are inherently linked, yet the species-specific characteristics of vegetation can do much to promote or inhibit tidal marsh resilience. While our results demonstrate the value of incorporating vegetation and channel structure into numerical models, they do not help to decipher the unexplained source of exported sediments we observed during our field campaign.

Our modelling efforts are an attempt to better understand how to promote vertical accretion in restored tidal marshes. Tidal marsh ecosystems are dynamic and can be difficult to simplify in a model. We sought to isolate the contribution of channel morphology, vegetation, tidal symmetry, and time in determining marsh evolution. If validated in other marshes, our models could help to develop best practices for conserving and restoring coastal ecosystems.

Conclusions

Understanding the factors that most significantly affect tidal marsh formation and degradation are vital to improving the resilience of coastal wetlands. In this research, we used field observations in conjunction with numerical models to show how vegetation and channel morphology effect flood-ebb dominance in an idealized tidal marsh. In-situ measurements of tides and *SSC* showed that our observed system is characterized by an asymmetric ebb tide with ebb dominance (Fig. 7), suggesting that erosion and sea-level rise are likely to become a more exaggerated and confounding threat to restored tidal marshes in the Chesapeake Bay over time. In-situ measurement of tides and *SSC* allowed us to compare the marsh's current,

ebb dominant state and its tidal asymmetry to our modelled systems. Coupling hydrodynamic and geomorphic numerical models is still relatively new but immensely powerful for isolating variable effects. Our model showed that stem density affects flood tides more than it does ebb tides, but that emergent vegetation more significantly reduced current velocities. *SSC* was equally influenced by vegetation density and height, and sediment was prone to fall out as water slowed down when passing through tall, dense vegetation. Channel geometry had a lesser influence on sediment retention than did vegetation; shallow, wide channels distributed water over a greater surface area leading to lower velocities and enhanced sediment trapping by vegetation when compared to deep, narrow channels that led to scouring (Fig. 10). Lastly, our numerical model showed that tidal symmetry did not influence flood tide velocity in shallow, wide channels or narrow, deep channels.

If Poplar Island is representative of tidal marshes throughout the Chesapeake Bay, greater emphasis needs to be placed on channel design and the important effect that robust vegetation has in promoting sediment retention. Improving tidal marsh modelling accuracy and precision is more important than ever in the face of rapidly rising sea levels. A recent economic analysis found that the cost of restoring marine ecosystems ranges between $150,000-400,000 USD per hectare (Bayraktarov et al., 2016). Our numerical models show the importance of coupling biotic and abiotic factors while emphasizing sediment aggregation effects in tidal marsh restoration. Our investigation highlights the importance of constructing model systems prior to beginning restoration efforts to maximize success in creating resilient tidal marshes.

Acknowledgments

We would like to thank Maryland Sea Grant for providing the opportunity to conduct research with the University of Maryland Center for Environmental Science at Horn Point Laboratory. We would like to thank the two reviewers who provided amazingly detailed feedback on our manuscript and provided an invaluable service to us. We would also like to thank the staff of the Maryland Environmental Service (MES) from the Paul S. Sarbanes Ecosystem Restoration Project at Poplar Island who constantly worked with us to schedule transportation, and Maryland Port Administration and USACE for allowing us permission to work on such a unique project. This study was supported by NSF grant OCE-1262374, and the Maryland Port Administration.

References

Anderson, M.E. and Smith, J.M., 2014. Wave attenuation by flexible, idealized salt marsh vegetation. Coastal Engineering, 83, pp.82-92. Assessment, M.E., 2005. Dryland Systems.

Baptist MJ. 2005. Modelling floodplain biogeomorphology.

Barbier EB, Hacker SD, Kennedy C, Koch EW, Stier AC, Silliman BR. 2011. The value of estuarine and coastal ecosystem services. Ecological Monographs 81 : 169–193. DOI: 10.1890/10-1510.1

Baustian JJ, Mendelssohn IA, Hester MW. 2012. Vegetation's importance in regulating surface elevation in a coastal salt marsh facing elevated rates of sea level rise. Global Change Biology 18 : 3377–3382. DOI: 10.1111/j.1365-2486.2012.02792.x

Bayraktarov E, Saunders MI, Abdullah S, Mills M, Beher J, Possingham HP, Mumby PJ, Lovelock CE. 2016. The cost and feasibility of marine coastal restoration. Ecological Applications 26 : 1055–1074. DOI: 10.1890/15-1077

Belliard J-P, Di Marco N, Carniello L, Toffolon M. 2016. Sediment and vegetation spatial dynamics facing sea-level rise in microtidal salt marshes: Insights from an ecogeomorphic model. Advances in Water Resources 93 : 249–264. DOI: 10.1016/j.advwatres.2015.11.020

Bernhardt, J.R. and Leslie, H.M., 2013. Resilience to climate change in coastal marine ecosystems.

Blum MJ, Jun Bando K, Katz M, Strong DR. 2007. Geographic structure, genetic diversity and source tracking of Spartina alterniflora. Journal of Biogeography 34 : 2055–2069. DOI: 10.1111/j.1365-2699.2007.01764.x

Boesch, D.F. and Turner, R.E., 1984. Dependence of fishery species on salt marshes: the role of food and refuge. Estuaries, 7(4), pp.460-468.

Bradshaw AD. 1984. Ecological principles and land reclamation practice. Landscape Planning 11 : 35–48. DOI: 10.1016/0304-3924(84)90016-9

Brown JM, Davies AG. 2010. Flood/ebb tidal asymmetry in a shallow sandy estuary and the impact on net sand transport. Geomorphology 114 : 431–439. DOI: 10.1016/j.geomorph.2009.08.006

Bryan KR, Nardin W, Mullarney JC, Fagherazzi S. 2017. The role of cross-shore tidal dynamics in controlling intertidal sediment exchange in mangroves in Cù Lao Dung, Vietnam. Continental Shelf Research 147 : 128–143. DOI: 10.1016/j.csr.2017.06.014

Carr J, Mariotti G, Fahgerazzi S, McGlathery K and Wiberg P. 2018. Exploring the Impacts of Seagrass on Coupled Marsh-Tidal Flat Morphodynamics. Front. Environ. Sci. 6:92. DOI: 10.3389/fenvs.2018.00092

Craft C, Clough J, Ehman J, Joye S, Park R, Pennings S, Guo H, Machmuller M. 2009. Forecasting the effects of accelerated sea-level rise on tidal marsh ecosystem services. Frontiers in Ecology and the Environment 7 : 73–78. DOI: 10.1890/070219

Crosby SC, Sax DF, Palmer ME, Booth HS, Deegan LA, Bertness MD, Leslie HM. 2016. Salt marsh persistence is threatened by predicted sea-level rise. Estuarine, Coastal and Shelf Science 181 : 93–99. DOI: 10.1016/j.ecss.2016.08.018

Deegan, L.A., Johnson, D.S., Warren, R.S., Peterson, B.J., Fleeger, J.W., Fagherazzi, S. and Wollheim, W.M., 2012. Coastal eutrophication as a driver of salt marsh loss. Nature, 490(7420), p.388.

Deines KL. 1999. Backscatter estimation using Broadband acoustic Doppler current profilers. presented at the Proceedings of the IEEE Sixth Working Conference on Current Measurement (Cat. No.99CH36331). 249–253 pp. March

Elschot K, Bouma T, Temmerman S, Bakker JP. 2013. Effects of long-term grazing on sediment deposition and salt-marsh accretion rates. Estuarine coastal and shelf science 133 : 109–115. DOI: 10.1016/j.ecss.2013.08.021

Fagherazzi, S., Kirwan, M.L., Mudd, S.M., Guntenspergen, G.R., Temmerman, S., D'Alpaos, A., van de Koppel, J., Rybczyk, J.M., Reyes, E., Craft, C. and Clough, J., 2012. Numerical models of salt marsh evolution: Ecological, geomorphic, and climatic factors. Reviews of Geophysics, 50(1).

Fourqurean JW et al. 2012. Seagrass ecosystems as a globally significant carbon stock. Nature Geoscience 5 : 505–509. DOI: 10.1038/ngeo1477

Fisher FH, Simmons VP. 1977. Sound absorption in sea water. The Journal of the Acoustical Society of America 62 : 558–564. DOI: 10.1121/1.381574

Gartner JW. 2004. Estimating suspended solids concentrations from backscatter intensity measured by acoustic Doppler current profiler in San Francisco Bay, California. Marine Geology 211 : 169–187. DOI: 10.1016/j.margeo.2004.07.001

Glick P, Clough J, Nunley B. 2008. Sea-Level Rise and Coastal Habitats in the Chesapeake Bay Region. National Wildlife Federation

Heiri O, Lotter AF, Lemcke G. 2001. Loss on ignition as a method for estimating organic and carbonate content in sediments: reproducibility and comparability of results. Journal of Paleolimnology 25 : 101–110. DOI: 10.1023/A:1008119611481

Holdaway GP, Thorne PD, Flatt D, Jones SE, Prandle D. 1999. Comparison between ADCP and transmissometer measurements of suspended sediment concentration. Continental Shelf Research 19 : 421–441. DOI: 10.1016/s0278-4343(98)00097-1

Kearney WS, Fagherazzi S. 2016. Salt marsh vegetation promotes efficient tidal channel networks. Nature Communications 7 : 12287. DOI: 10.1038/ncomms12287

Kelley D, Richards C. 2017. oce: Analysis of Oceanographic Data. R package version 0.9-21. [online] Available from: https://CRAN.R-project.org/package=oce

Kelly W. 2017. Paul S. Sarbanes Ecosystem Restoration Project at Poplar Island. In Engineering for Sustainable Communities: Principles and Practices (pp. 411-417).

Kent J. 2015. Water level variations at Poplar Island, MD. Rep. NOAA NOS CO-OPS 076, Silver Spring, MD, 35 pp, U. S. Department of Commerce.

Kirwan ML, Murray AB. 2007. A coupled geomorphic and ecological model of tidal marsh evolution. Proceedings of the National Academy of Sciences of the United States of America 104 : 6118–6122. DOI: 10.1073/pnas.0700958104

Leonard, L.A. and Croft, A.L., 2006. The effect of standing biomass on flow velocity and turbulence in Spartina alterniflora canopies. Estuarine, Coastal and Shelf Science, 69(3-4), pp.325-336.

Leonard, L.A. and Luther, M.E., 1995. Flow hydrodynamics in tidal marsh canopies. Limnology and oceanography, 40(8), pp.1474-1484.

Lera S., W. Nardin, L. Sanford, C. Palinkas and R. Guercio (2019). The impact of submersed aquatic vegetation on the development of river mouth bars. Earth Surface Processes and Landforms, doi:10.1002/esp.4585

Lesser GR, Roelvink DJA, van Kester JATM, Stelling G. 2004. Development and Validation of a Three-Dimensional Morphological Model. Coastal Engineering 51: 883–915. DOI: 10.1016/j.coastaleng.2004.07.014

Lohrmann A. 2001. Monitoring sediment concentration with acoustic backscattering instruments. Technical Note 003 : pp 5., Nortek AS, Rud Norway

Mazda Y, Wolanski E, King B, Sase A, Ohtsuka D, Magi M. 1997. Drag force due to vegetation in mangrove swamps. Mangroves and Salt Marshes 1 : 193–199. DOI: 10.1023/A:1009949411068

Moffett KB, Robinson DA, Gorelick SM. 2010. Relationship of Salt Marsh Vegetation Zonation to Spatial Patterns in Soil Moisture, Salinity, and Topography. Ecosystems 13 : 1287–1302. DOI: 10.1007/s10021-010-9385-7

Möller I et al. 2014. Wave attenuation over coastal salt marshes under storm surge conditions. Nature Geoscience 7 : 727–731. DOI: 10.1038/ngeo2251

Monismith, S., Jones, N., Bela, M., Nidzieko, N., Paytan, A., Misra, G. and Street, J., 2005. Hydrodynamics and sediment dynamics in Elkhorn Slough. A report to Monterey Bay Sanctuary Foundation.

Morris JT, Sundareshwar PV, Nietch CT, Kjerfve B, Cahoon DR. 2002. Responses of Coastal Wetlands to Rising Sea Level. Ecology 83 : 2869. DOI: 10.2307/3072022

Mudd SM, Fagherazzi S, Morris JT, Furbish DJ. 2004. Flow, Sedimentation, and Biomass Production on a Vegetated Salt Marsh in South Carolina: Toward a Predictive Model of Marsh Morphologic and Ecologic Evolution. In The

Ecogeomorphology of Tidal Marshes , Fagherazzi S, Rcorani, and Blum LK (eds). American Geophysical Union; 165–188. [online] Available from: http://onlinelibrary.wiley.com/doi/10.1029/CE059p0165/summary (Accessed 13 February 2018)

Nardin W., L. Larsen, S. Fagherazzi and P. Wiberg, 2018. Tradeoffs among hydrodynamics, sediment fluxes and vegetation community in the Virginia Coast Reserve, USA, Estuarine, Coastal and Shelf Science, doi: 10.1016/j.ecss.2018.06.009.

Nardin W, Edmonds DA, Fagherazzi S. 2016. Influence of vegetation on spatial patterns of sediment deposition in deltaic islands during flood. Advances in Water Resources 93: 236–248. DOI: 10.1016/j.advwatres.2016.01.001

Nardin W., D. A. Edmonds and S. Fagherazzi, Influence of vegetationon spatial patterns of sediment deposition in deltaic islands during flood, Advances in Water Resources (2016) doi: 10.1016/j.advwatres.2016.01.001.

Nardin W, Mariotti G, Edmonds DA, Guercio R, Fagherazzi S. 2013. Growth of river mouth bars in sheltered bays in the presence of frontal waves. Journal of Geophysical Research: Earth Surface 118 : 872–886. DOI: 10.1002/jgrf.20057

National Research Council. 2012. Sea-Level Rise for the Coasts of California, Oregon, and Washington: Past, Present, and Future [online] Available from: https://www.nap.edu/catalog/13389/sea-level-rise-for-the-coasts-of-california-oregon-and-washington (Accessed 13 February 2018)

Parry, M., Parry, M.L., Canziani, O., Palutikof, J., Van der Linden, P. and Hanson, C. eds., 2007. Climate change 2007-impacts, adaptation and vulnerability:

Working group II contribution to the fourth assessment report of the IPCC (Vol. 4). Cambridge University Press.

Priestas AM, Mariotti G, Leonardi N, Fagherazzi S. 2015. Coupled Wave Energy and Erosion Dynamics along a Salt Marsh Boundary, Hog Island Bay, Virginia, USA. Journal of Marine Science and Engineering 3 : 1041–1065. DOI: 10.3390/jmse3031041

Sallenger AH, Doran KS, Howd PA. 2012. Hotspot of accelerated sea-level rise on the Atlantic coast of North America. Nature Climate Change 2 : 884–888. DOI: 10.1038/nclimate1597

Staver LW, Cornwell JC, Stevenson JC, and Owens M. (2018) Paul S. Sarbanes Ecosystem Restoration Project at Poplar Island Wetland Cells Monitoring Program: 2016–2017 Studies to Address Sustainability in the Poplar Island Marshes. #TS-714-18. University of Maryland Center for Environmental Science, Cambridge, MD

Stevenson JC, Cornwell JC, Staver L, and Owens M. (2013) Paul S. Sarbanes Ecosystem Restoration Project at Poplar Island Wetland Cells Monitoring Program: 2011 Studies to Address Sea-Level Rise, Marsh Dieback and Silicon-Related Issues, Final Report. University of Maryland Center for Environmental Science, Horn Point Laboratory

Suding KN. 2011. Toward an Era of Restoration in Ecology: Successes, Failures, and Opportunities Ahead. Annual Review of Ecology, Evolution, and Systematics 42 : 465–487. DOI: 10.1146/annurev-ecolsys-102710-145115

Temmerman S, Bouma TJ, Govers G, Wang ZB, De Vries MB, Herman PMJ. 2005. Impact of vegetation on flow routing and sedimentation patterns: Three-

dimensional modeling for a tidal marsh. Journal of Geophysical Research-Earth Surface 110 DOI: 10.1029/2005jf000301

Van Rijn LC. 1993. Principles of sediment transport in rivers, estuaries and coastal seas. Aqua publications Amsterdam - I11. with ref. ISBN 90-800356-2-9 bound NUGI 816/831

Ward LG, Michael Kemp W, Boynton WR. 1984. The influence of waves and seagrass communities on suspended particulates in an estuarine embayment. Marine Geology 59 : 85–103. DOI: 10.1016/0025-3227(84)90089-6

Wen-Cheng L, Ming-Hsi H, Chi-Fang W. 2003. Modeling of Flow Resistance in Mangrove Swamp at Mouth of Tidal Keelung River, Taiwan. Journal of Waterway, Port, Coastal, and Ocean Engineering 129 : 86–92. DOI: 10.1061/(ASCE)0733-950X(2003)129:2(86)

Wu Y, Falconer RA, Struve J. 2001. Mathematical modelling of tidal currents in mangrove forests. Environmental Modelling and Software 16 : 19–29. DOI: 10.1016/S1364-8152(00)00059-1

Name	Latitude	Longitude	Distance from seabed (m)	Start time	End time	Sampling interval (s)	Cell size (cm)	Resolution (MHz)
Cul	38°46'15.38"	76°22'35.89"	0.150	7/7/17 12:00	7/12/17 13:45	180	5	2
Cul2	38°46'15.38"	76°22'35.89"	0.150	7/19/17 12:00	7/21/17 10:00	180	5	2
NE	38°46'22.30"	76°22'34.55"	0.150	7/7/17 12:00	7/12/17 13:45	180	10	2
SE	38°46'10.93"	76°22'41.83"	0.100	7/7/17 12:00	7/12/17 13:45	180	25	1
MC	38°46'18.69"	76°22'41.93"	0.150	7/19/17 12:00	7/21/17 10:00	180	10	2
SC	38°46'15.84"	76°22'44.13"	0.100	7/19/17 12:00	7/21/17 10:00	180	25	1

Table 1: Details of ADCP deployment locations

Run ID	Channel width [m]	Channel depth [m]	h_v [m]	n [1/m]
R01	24	0.25	0.1	2
R02	24	0.25	0.1	6
R03	24	0.25	0.1	10
R04	24	0.25	1.6	2
R05	24	0.25	1.6	6
R06	24	0.25	1.6	10
R07	6	0.80	0.1	2
R08	6	0.80	0.1	6
R09	6	0.80	0.1	10
R10	6	0.80	1.6	2
R11	6	0.80	1.6	6
R12	6	0.80	1.6	10
R13	12	0.83	0.1	2
R14	12	0.83	0.1	6
R15	12	0.83	0.1	10
R16	12	0.83	1.6	2
R17	12	0.83	1.6	6
R18	12	0.83	1.6	10

Table 2a: Numerical model configurations with varying initial channel morphology and vegetation characteristics. h_v shows vegetation height in meters and n refers to stem densities.

Run ID	Channel width [m]	Channel depth [m]	h_v [m]	n [1/m]
R19	24	0.25	0.1	4
R20	24	0.25	0.1	8
R21	24	0.25	1.6	4
R22	24	0.25	1.6	8
R23	6	0.80	0.1	4
R24	6	0.80	0.1	8
R25	6	0.80	1.6	4
R26	6	0.80	1.6	8
R27	12	0.83	0.1	4
R28	12	0.83	0.1	8
R29	12	0.83	1.6	4
R30	12	0.83	1.6	8
R31	18	0.32	0.1	2
R32	18	0.32	0.1	4
R33	18	0.32	0.1	6
R34	18	0.32	0.1	8
R35	18	0.32	0.1	10
R36	18	0.32	1.6	2
R37	18	0.32	1.6	4
R38	18	0.32	1.6	6
R39	18	0.32	1.6	8
R40	18	0.32	1.6	10
R41	24	0.25	no veg	
R42	6	0.80	no veg	
R43	12	0.83	no veg	
R44	18	0.32	no veg	

Table 2b: Model configurations used to calculate the sediment dynamic ratios R_c and R_a.

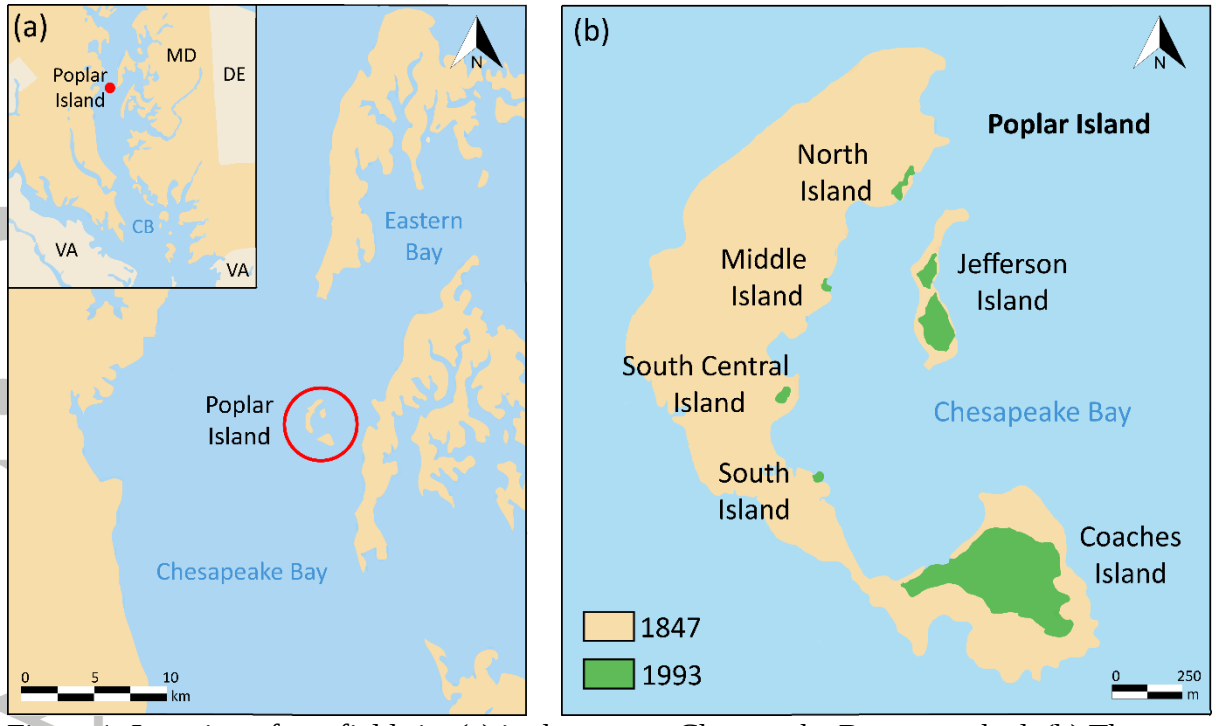

Figure 1: Location of our field site (a) in the greater Chesapeake Bay watershed. (b) The historic extent and reduction of Poplar Island between 1847 and 1993.

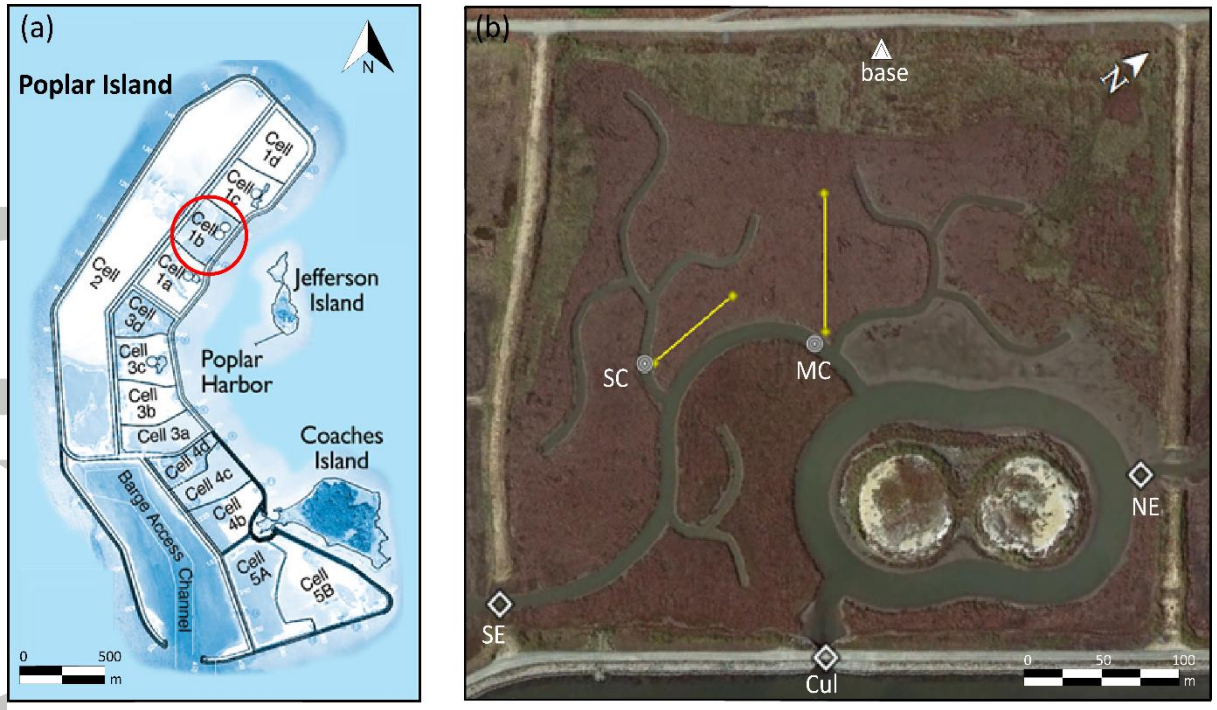

Figure 2: Poplar Island today (2005) (a) where marshes are being restored in cells on the eastern portion of the island. We focus on cell 1B (b) where diamonds denote our 1st ADCP deployment locations, circles indicate the 2nd deployment locations, vegetation and sediment line transects are shown in yellow and the triangle identifies the GPS base location (courtesy of Google Earth and U.S. Army Corps of Engineers).

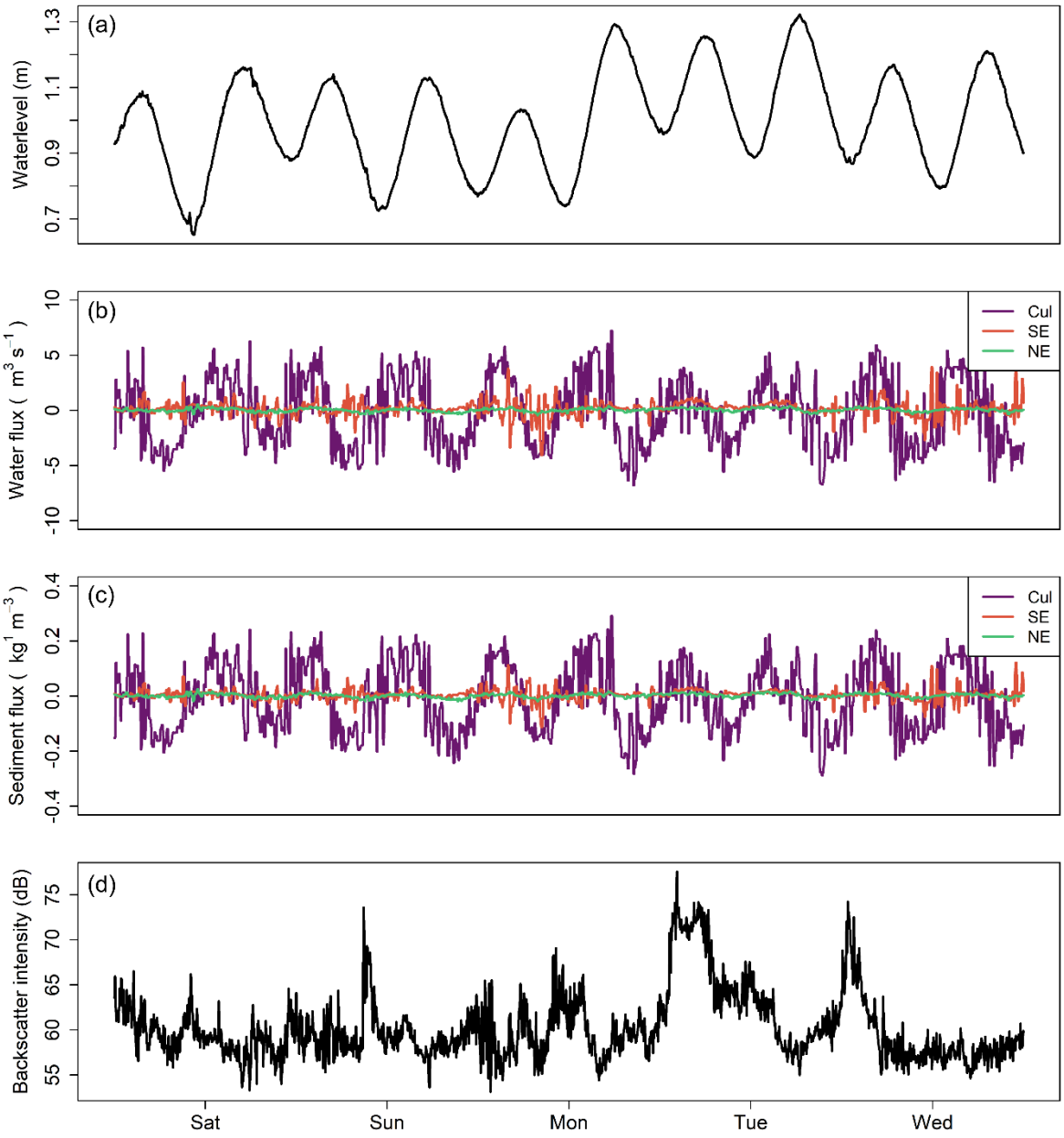

Figure 3: Time series of site observations collected during 1st deployment of ADCPs during July 2017. (a) Water level data collected and from ADCP unit inside the culvert. (b) Instantaneous water fluxes smoothed by a moving median at each channel inlet. (c) Instantaneous sediment fluxes smoothed by a moving median at each channel inlet. (d) Culvert backscatter intensity converted to decibels for sediment flux calculations.

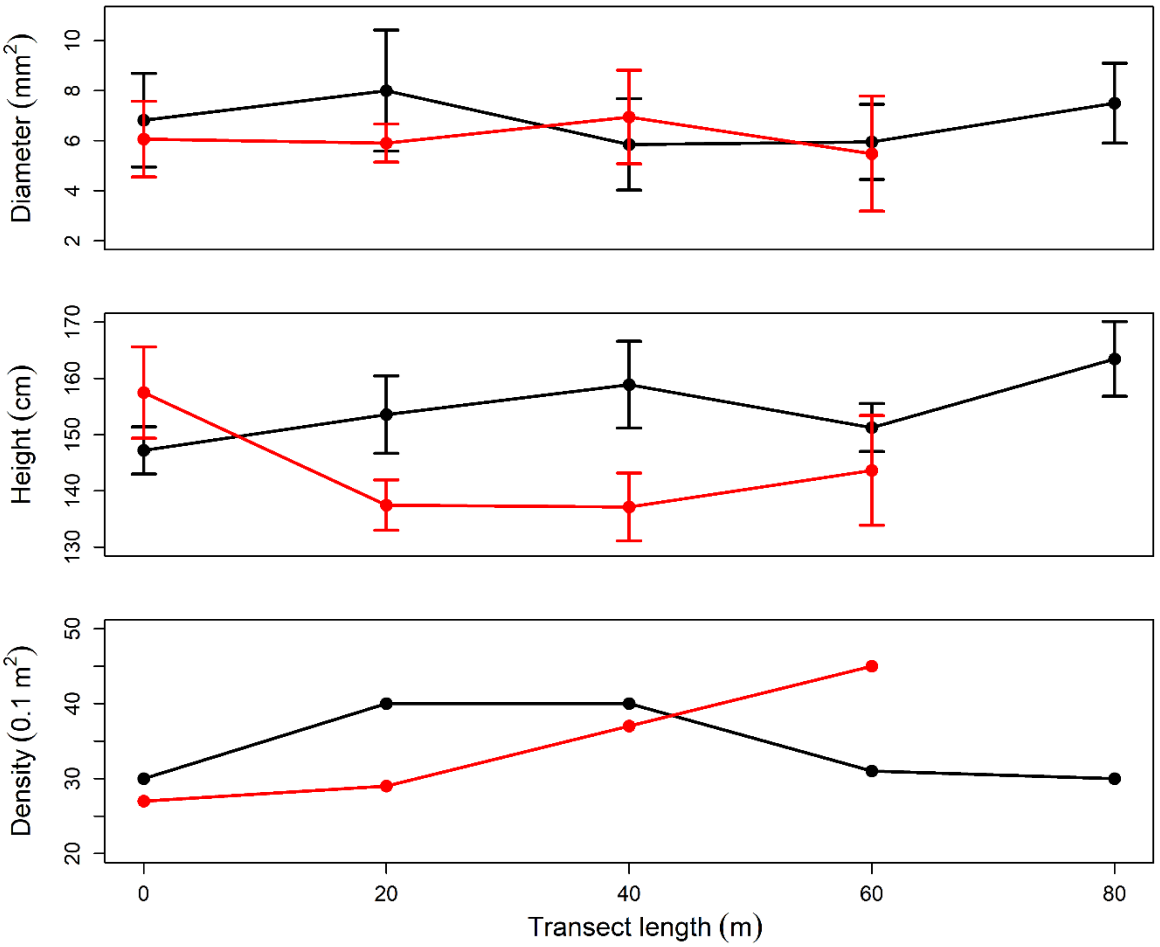

Figure 4: Vegetation characteristics taken along two transects. The black line represents transect 1 (80 m), while the red line shows transect 2 (60 m). Error bars show +/- 1 standard deviation. (a) Stem diameter taken at 15 cm above the ground. (b) Mean height of tallest five grasses inside the quadrate. (c) Total density of stems inside the quadrat.

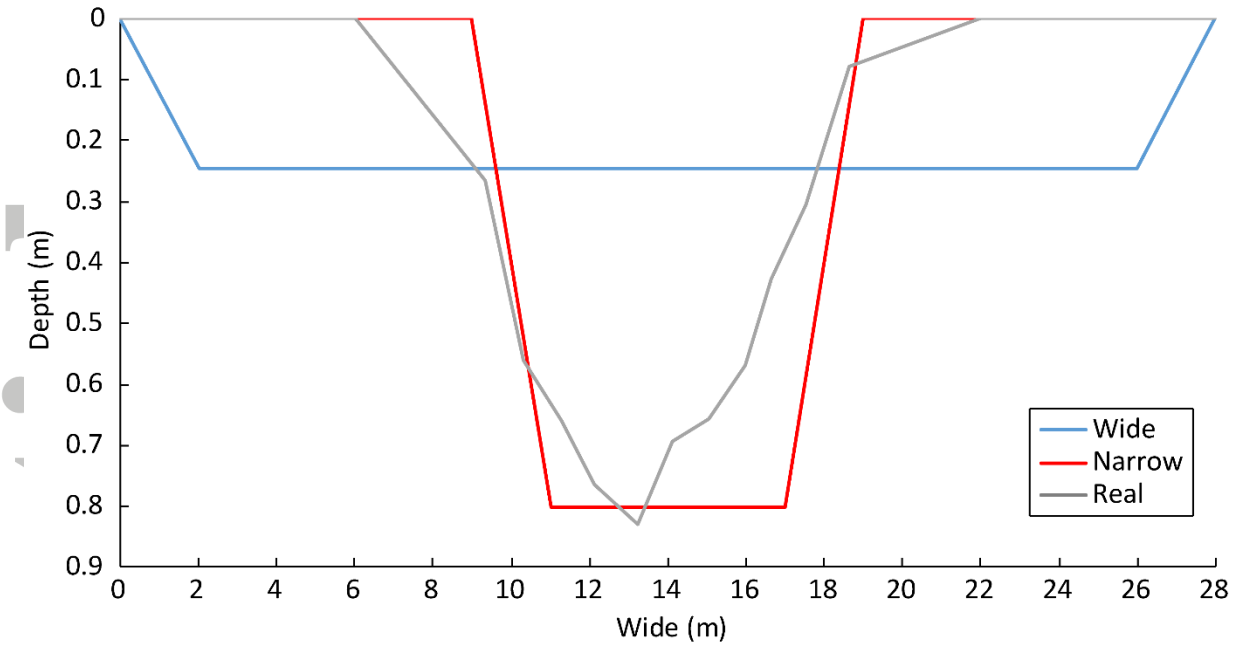

Figure 5: Model domain grid with refinement (a), vegetated area and boundary condition (b) where the channel is in blue. Tidal reference conditions were based off NOAA observations in Cambridge, MD. (c) The blue line represents the predicted tide while the green line shows the verified tide.

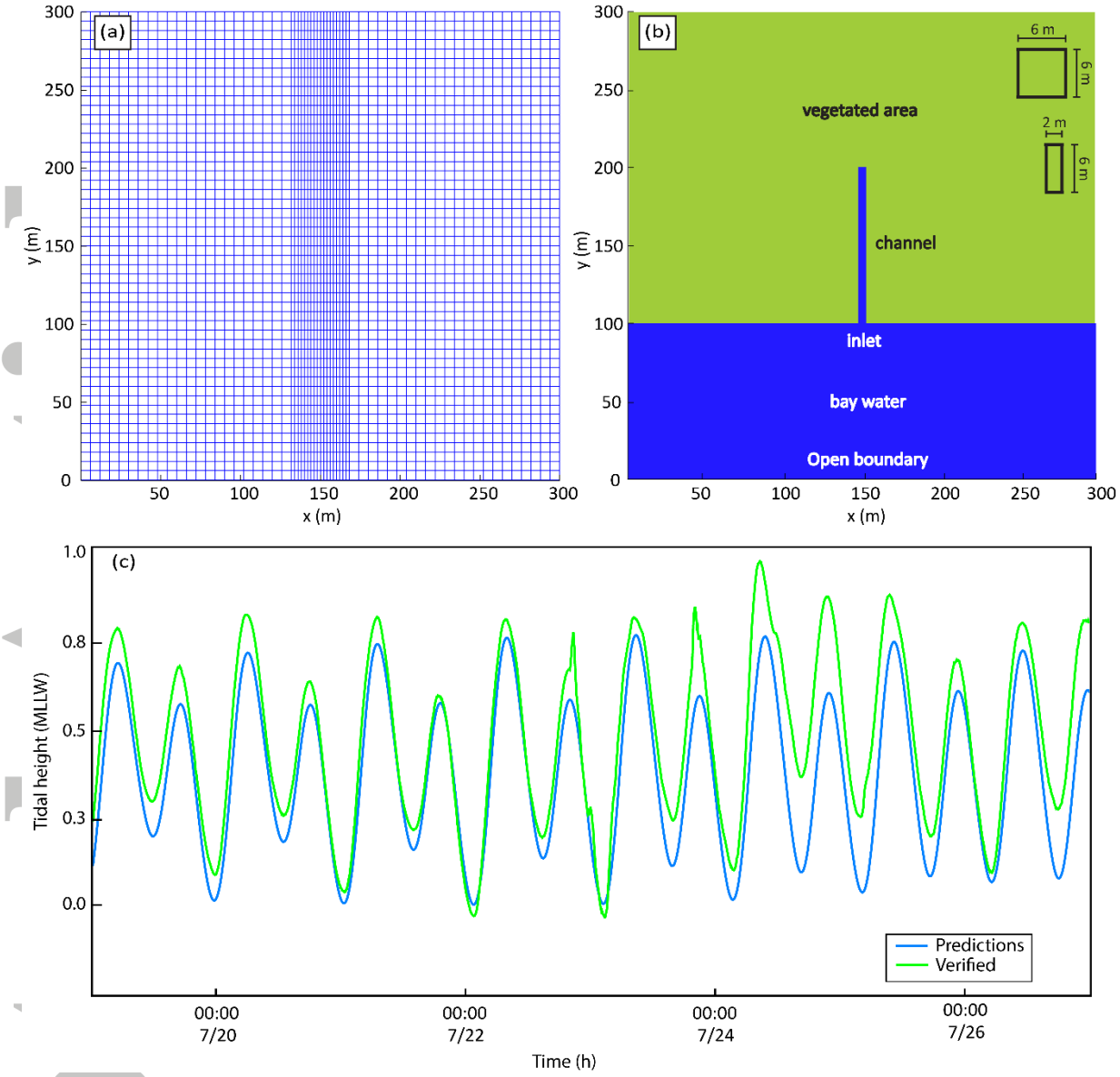

Figure 6: Varying channel configurations that were simulated in the numerical models. Where blue is the shallow, wide channel, red is the deep narrow channel and gray is the focal channel (SC) from Poplar Island.

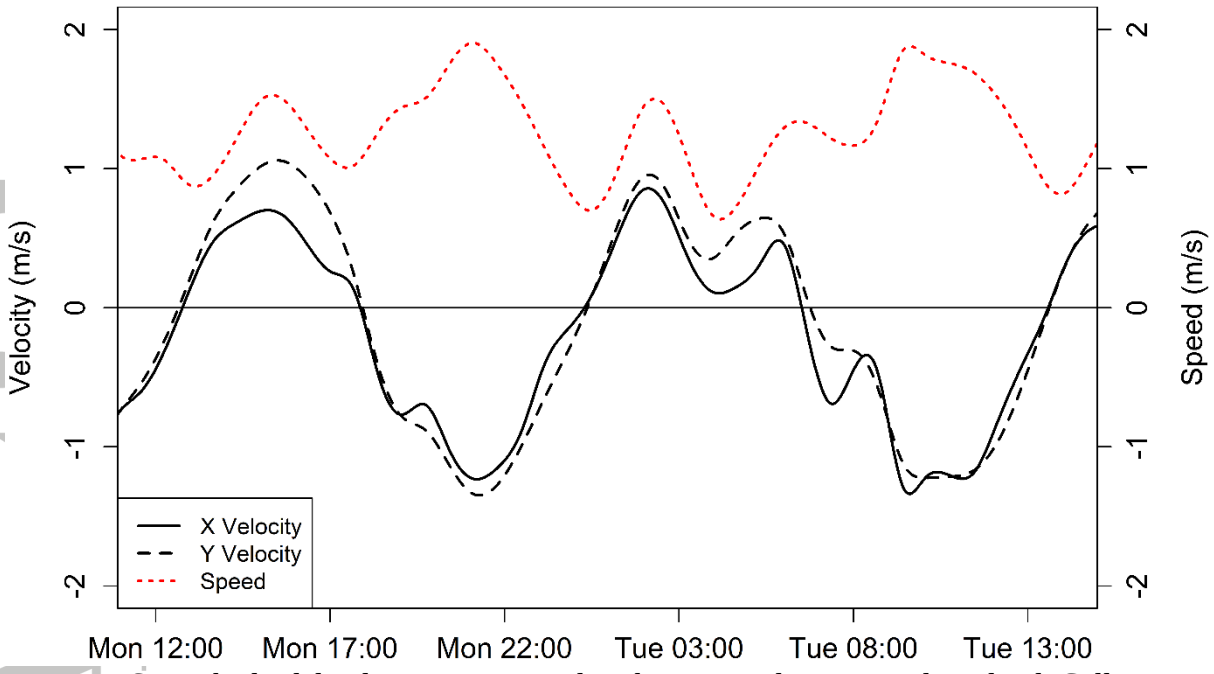

Figure 7: Smoothed tidal velocities measured in the main culvert at Poplar Island, Cell 1B. Positive velocities indicate a flood tide where speed values can be compared during peak flood and ebb tides.

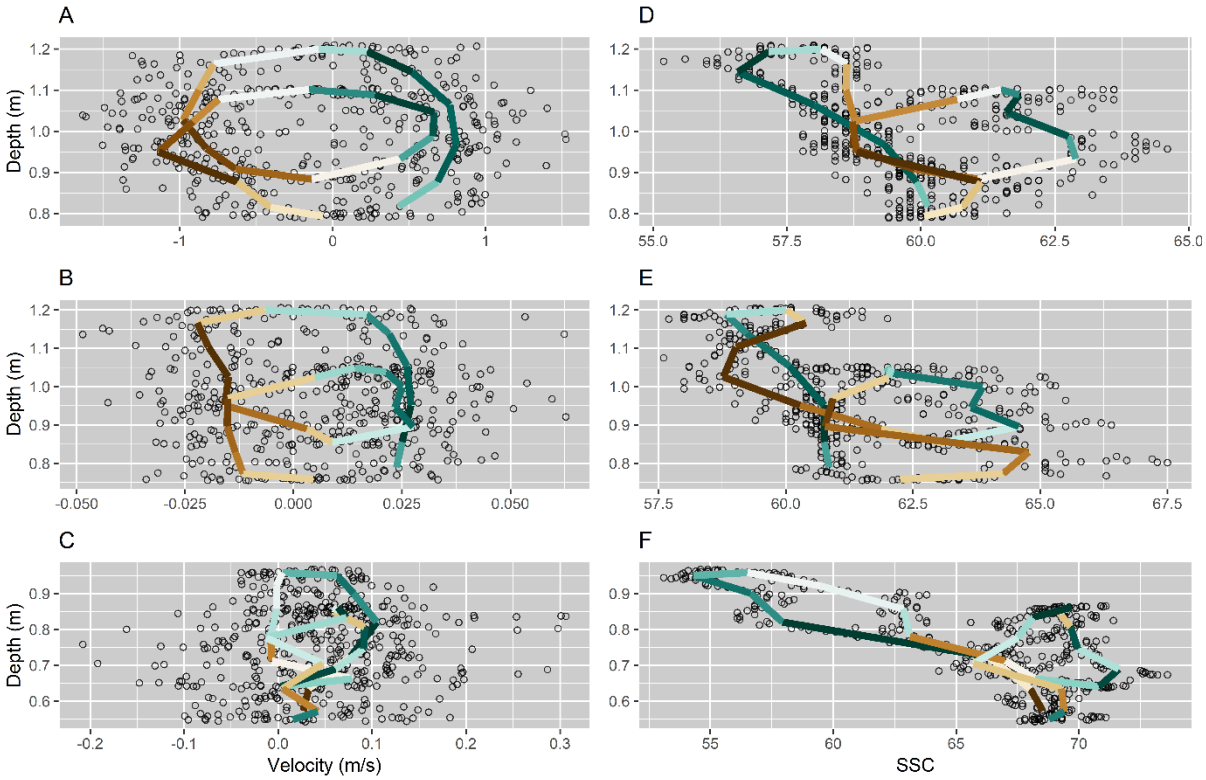

Figure 8: Tidal stages plot from the 1st deployment, where (a) shows velocities from the culvert paired with SSC (b) measured simultaneously. (c-d) depict the same observations for the northernmost inlet, and (e-f) for the southern inlet. Hollow circles represent mean observations recorded at three-minute intervals over five days. Colored lines show mean hourly observations averaged over the same five-day period where blue lines signify flood tides and brown depicts ebb tides.

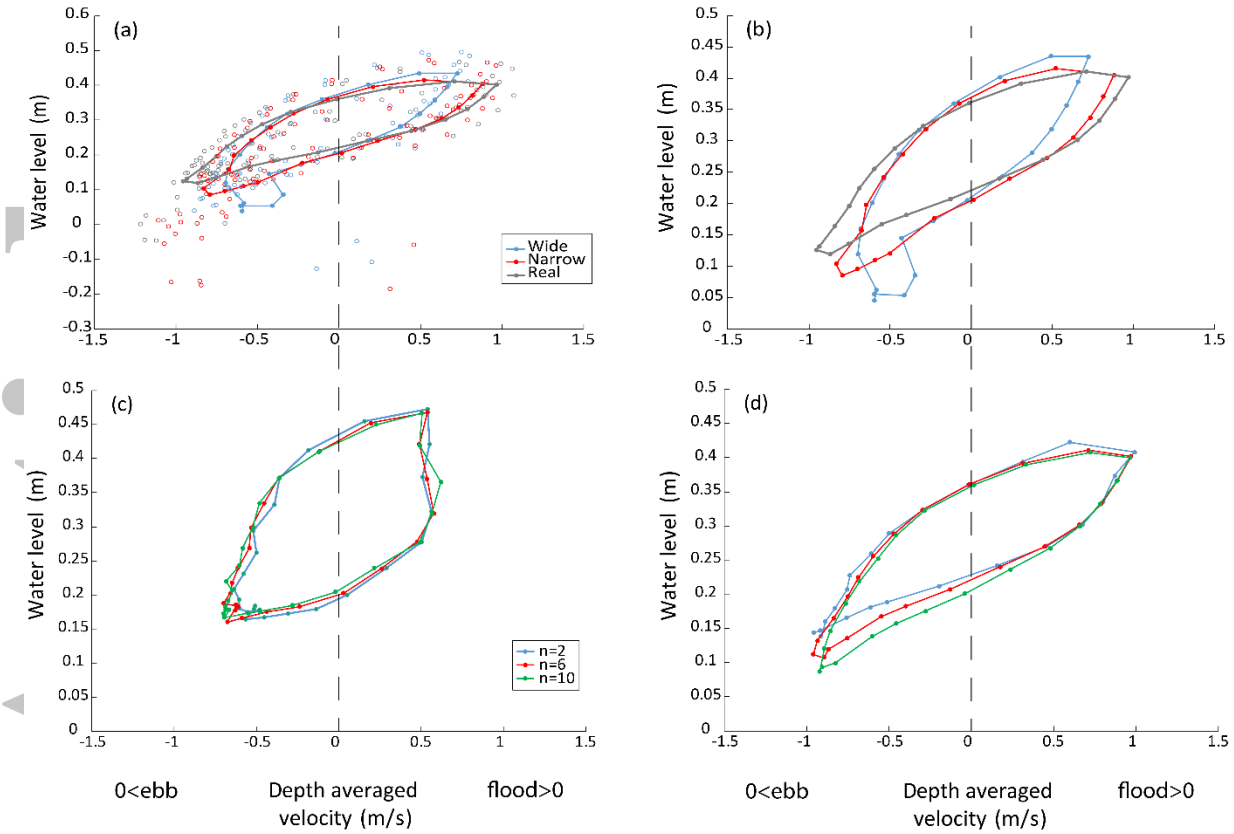

Figure 9: Flood-ebb dominance plots extracted from the numerical modelling output at the observation point with variation in channel shape (a-b), and stem density (c-d). The top panels show the same results: the unfilled circles represent the unaveraged outputs collected during the last 4 tidal cycles and were omitted from subsequent panels to increase clarity. The blue lines in a-b represent a shallow, wide channel, red is the deep, narrow channel, and grey is the real cross section. Vegetation in the top plots had uniform heights of 1.6 m and stem densities equal to 6 m-1 but varied in the lower plots with stem heights of 0.1 m (c) and density of 1.6 m (d). Where blue lines denote the lowest stem density (n = 2 m-1), red is moderate (n = 6 m-1), and green is high density (n = 10 m-1).

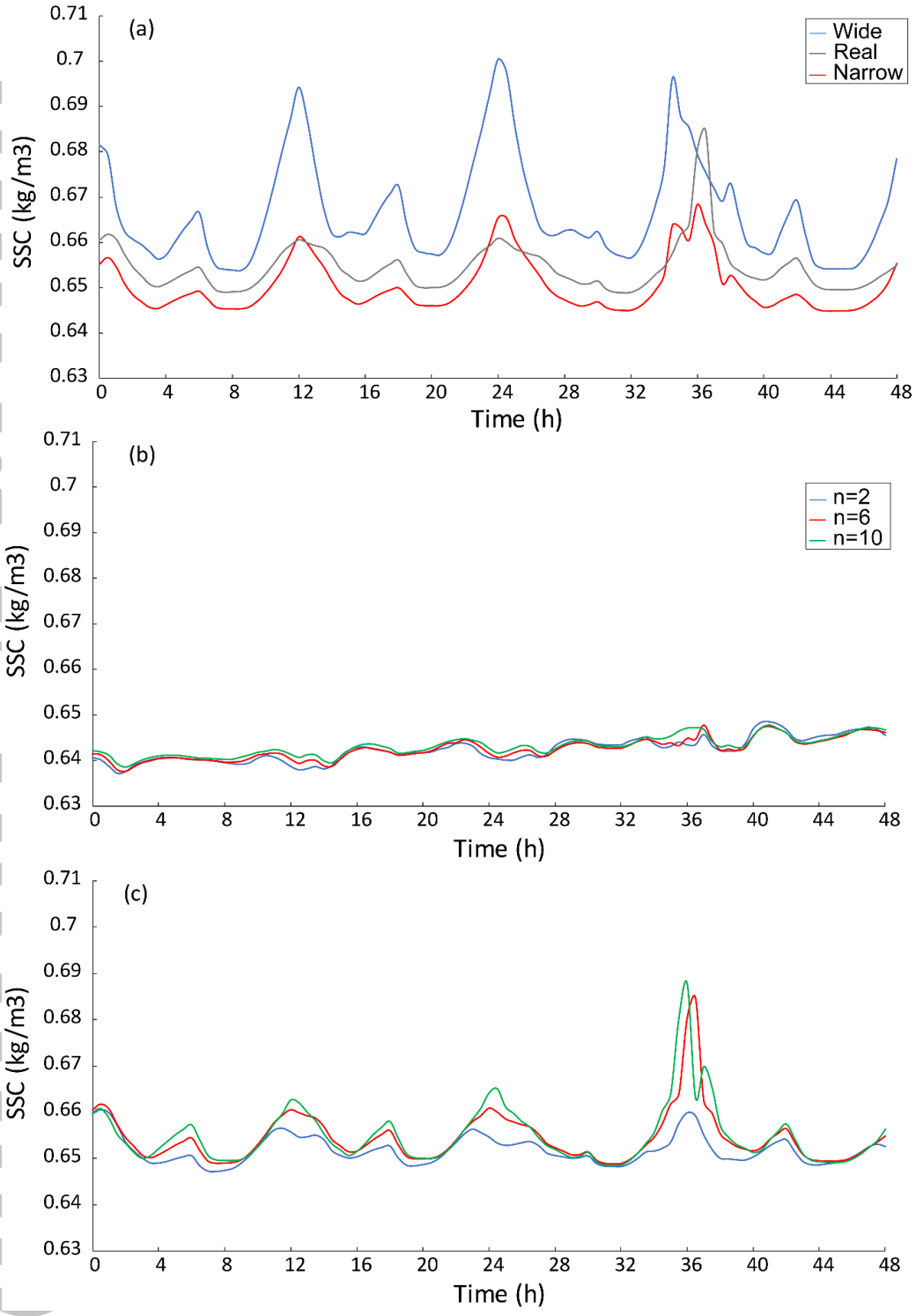

Figure 10: Suspended sediment concentration plots extracted from the numerical modelling results at the observation point. The top panel (a) display the data collected in 48 hr with shape variation. The blue dashed lines represent the shallow, wide channel configuration, the red lines the deep, narrow channel configuration and the grey line the real channel section taken from SC. The bottom panels display the vegetation variation with height stems of 0.1 m (b) or height stems of 1.6m (c) and density of n=2 m−1 (blue), n=6 m−1 (red) and n=10 m−1 (green).

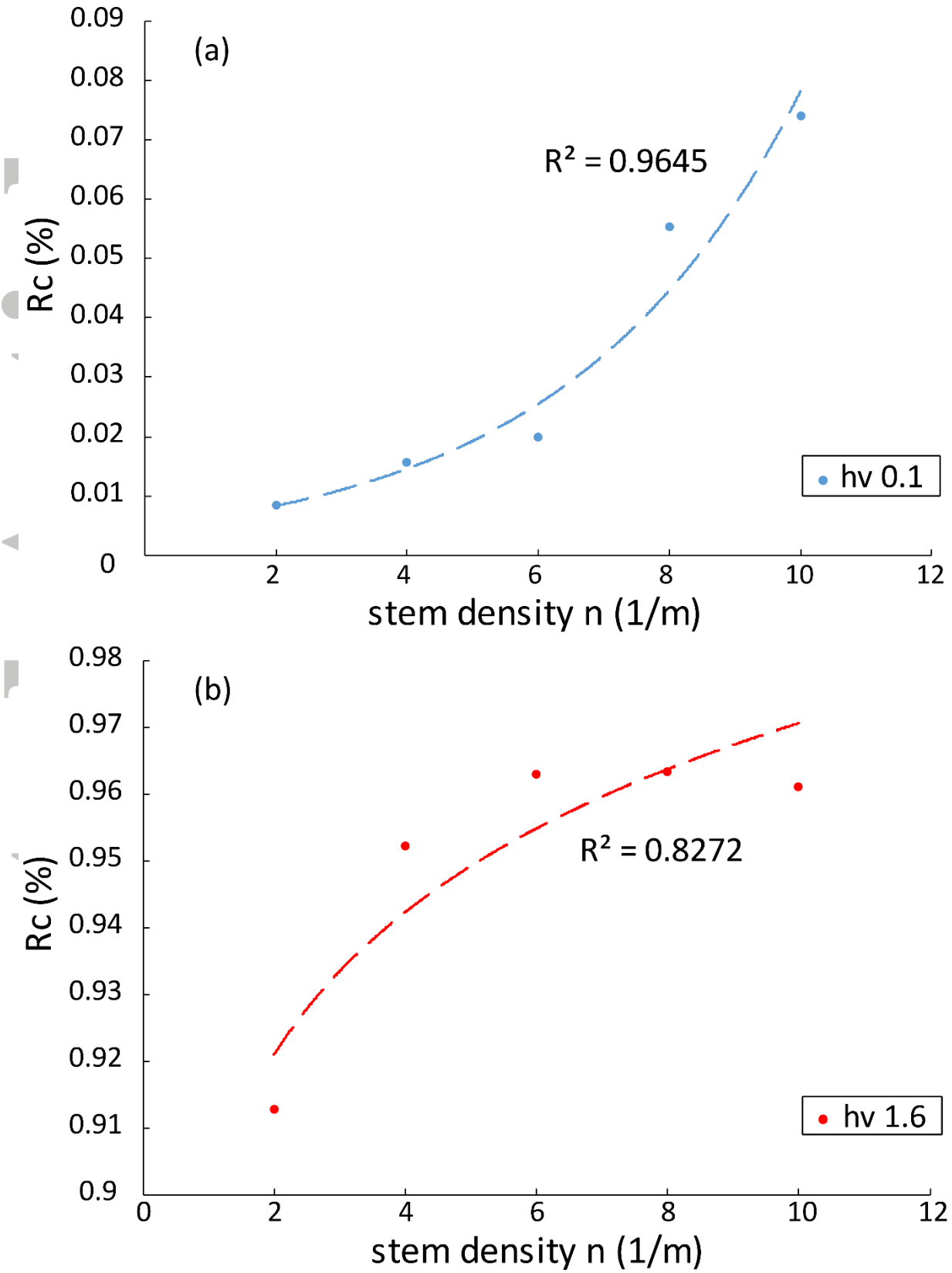

Figure 11: R_c coefficient at varying vegetation densities at channel SC. (a) Blue lines denote vegetation at a height of 0.1 m while (b) red lines show vegetation at 1.6 m. Trendlines are dashed.

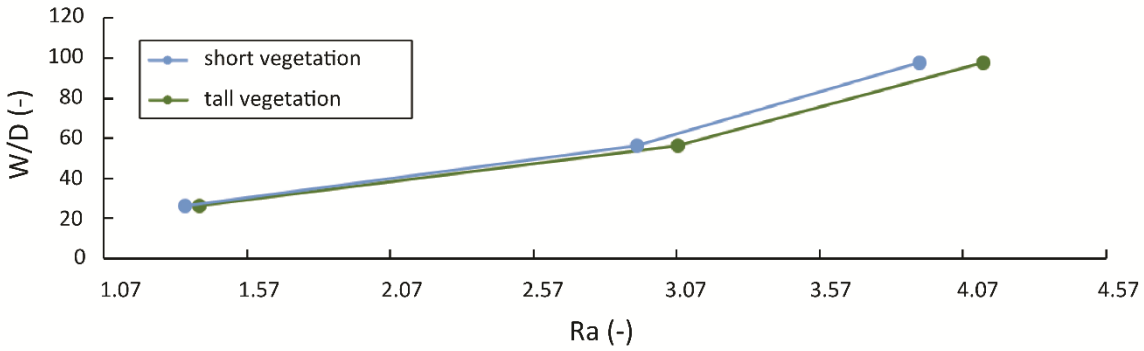

Figure 12: Accretion coefficient for differing vegetation volumes. Vegetation height at 0.1 m is shown in blue and 1.6 m is in green.